Pulse ENDOR studies on the radical pair P 700+· A 1·− and the photoaccumulated quinone acceptor A 1·− of photosystem I

ARTICLE *in* APPLIED MAGNETIC RESONANCE · MARCH 2004

Impact Factor: 1.17 · DOI: 10.1007/BF03166559 · Source: OAI

3 AUTHORS, INCLUDING:

Christian Teutloff
Freie Universität Berlin
48 PUBLICATIONS **831** CITATIONS

Appl. Magn. Reson. 26, 5–21 (2004)

Applied Magnetic Resonance

Pulse ENDOR Studies on the Radical Pair $P_{700}^{+\bullet}A_1^{\bullet-}$ and the Photoaccumulated Quinone Acceptor $A_1^{\bullet-}$ of Photosystem I

C. Teutloff[1], R. Bittl[2], and W. Lubitz[3]

[1] Max-Volmer-Laboratorium, Technische Universität Berlin, Berlin, Germany
[2] Institut fur Experimentalphysik, Freie Universität Berlin, Berlin, Germany
[3] Max-Planck-Institut fur Bioanorganische Chemie, Mülheim an der Ruhr, Germany

Received November 28, 2003

Abstract. The secondary acceptor A_1 of the electron transport chain(s) of photosystem (PS) I is a phylloquinone (vitamin K_1, VK_1). Pulse electron paramagnetic resonance and electron nuclear double resonance (ENDOR) experiments at X-band frequencies were performed on the photoaccumulated acceptor radical $A_1^{\bullet-}$ and the radical pair state $P_{700}^{+\bullet}A_1^{\bullet-}$ in PS I of *Thermosynechococcus elongatus*. The data obtained were compared with data from the respective radical anion of VK_1 in organic solvents. The unusual g tensor magnitude of $A_1^{\bullet-}$ is explained by the hydrophobic binding pocket of this radical. The hyperfine couplings and the spin (and charge) density distribution is very different for $A_1^{\bullet-}$ in PS I and $VK_1^{\bullet-}$ in frozen alcoholic solution. This is attributed to a rather strong one-sided hydrogen bond to $A_1^{\bullet-}$. The presence of a hydrogen bond to $A_1^{\bullet-}$ has only a minor effect on g. The hyperfine coupling constants of $A_1^{\bullet-}$ determined from the radical pair spectra deviate only slightly from those derived from photoaccumulated $A_1^{\bullet-}$ in PS I treated with dithionite at high pH. ENDOR resonances of the proton in a H bond were detected and an estimate of the strength and geometry of this bond to $A_1^{\bullet-}$ was obtained. The significance of the hydrogen bond and other (hydrophobic) interactions of A_1 with the surrounding are briefly discussed.

1 Introduction

In plants, algae and cyanobacteria the light-induced charge separation of photosynthesis occurs in two large membrane proteins, called photosystem I (PS I) and photosystem II (PS II). PS I catalyzes the electron transfer from plastocyanin (or cytochrome c_6) on the lumenal side to ferredoxin (or flavodoxin) on the stromal side of the membrane via an electron transport (ET) chain [1–3]. PS I from *Thermosynechococcus elongatus* was crystallized and an X-ray crystallographic structure at 0.25 nm resolution has recently been obtained [4]. The protein complex consists of 12 subunits that contain 96 chlorophyll *a* molecules, 22 carotenoids, three 4Fe4S centers and two phylloquinone (vitamin K_1, VK_1) molecules. The cofactors of the ET chain are arranged in two branches

as pairs of molecules related by a pseudo-C_2 axis. After light excitation an electron is donated from the primary donor P_{700}, a pair of chlorophylls, to monomeric chlorophyll *a* (acceptor A_0), phylloquinone (A_1) and the three FeS centers (F_X, F_A and F_B) [2]. It has been controversially discussed in the literature [5, 6] whether both pigment branches are actively involved in the ET (for a review see ref. 3).

Electron paramagnetic resonance (EPR) techniques have been widely applied to study the radical ions and radical pairs created in the light-induced ET process in PS I [7–12]. In this communication we focus on the PS I acceptor side, i.e., on the quinone radicals. The identification of the secondary electron acceptor A_1 with a quinone was first shown by transient EPR performed on the secondary radical pair $P_{700}^{\bullet+}A_1^{\bullet-}$, and later by EPR/ENDOR (electron nuclear double resonance) on the photoaccumulated radical $A_1^{\bullet-}$ [13–15]. Further support came from transient EPR experiments at 94 GHz [16, 17] and EPR at 283 GHz [18] that identified a radical with a *g*-anisotropy typical for a quinone anion radical [19, 20]. Excellent agreement of the EPR characteristics of $A_1^{\bullet-}$ in PS I and of $VK_1^{\bullet-}$ in polar (ether) solvents has recently been demonstrated [21].

An interesting feature of PS I is the very negative redox potential of all the constituents of the ET chain, e.g., the potential of the $A_1/A_1^{\bullet-}$-couple is estimated to about -800 mV [22, 23] as compared with that of $VK_1/VK_1^{\bullet-}$ in water of -170 mV (vs. normal hydrogen electrode, NHE) [24]. This large difference must be due to the specific protein surrounding of the quinone binding pocket. According to the crystal structure of PS I of *T. elongatus* the two quinones are in a very similar surrounding [4]. They are located in hydrophobic binding pockets in the psaA and the psaB subunit of the protein and probably interact both with the backbone N-H of a leucine (Leu A722 and Leu B706, respectively), which form one-sided hydrogen bonds to the oxygens (O_4) of $A_1^{\bullet-}$ (see Fig. 1). Furthermore, one tryptophan (Trp A697, Trp B677) is π-stacked to the quinone rings, distances range from 0.30 to 0.35 nm [2]. The electronic interaction of the Trp with $A_1^{\bullet-}$ has been demonstrated by electron spin echo envelope modulation (ESEEM) experiments [25].

The *g* tensor components of quinone radical anions are good indicators for the polarity of the radical's surrounding [20, 21, 26–29]. The *g* values obtained for $A_1^{\bullet-}$ in PS I show that the environment must be very hydrophobic in agreement with the information deduced from the X-ray crystallographic structure [2, 4]. The measured hyperfine couplings (hfc) of $A_1^{\bullet-}$ [15, 30] indicate, however, a very strong shift of spin density in this radical that could be caused by asymmetric hydrogen bonding (to O_4 of VK_1). Such a one-sided H bond has indeed been found in the X-ray structure (Fig. 1b). Obviously, this single H bond has no significant effect on the *g* tensor but profoundly affects the hfcs.

So far there has been no direct evidence, e.g., from ENDOR spectroscopy on D_2O exchanged samples, for the existence of such a H bond, since H-D exchange has been unsuccessful and the rich structure in the ENDOR spectra could not be fully interpreted. One of the problems is that the radical of the second-

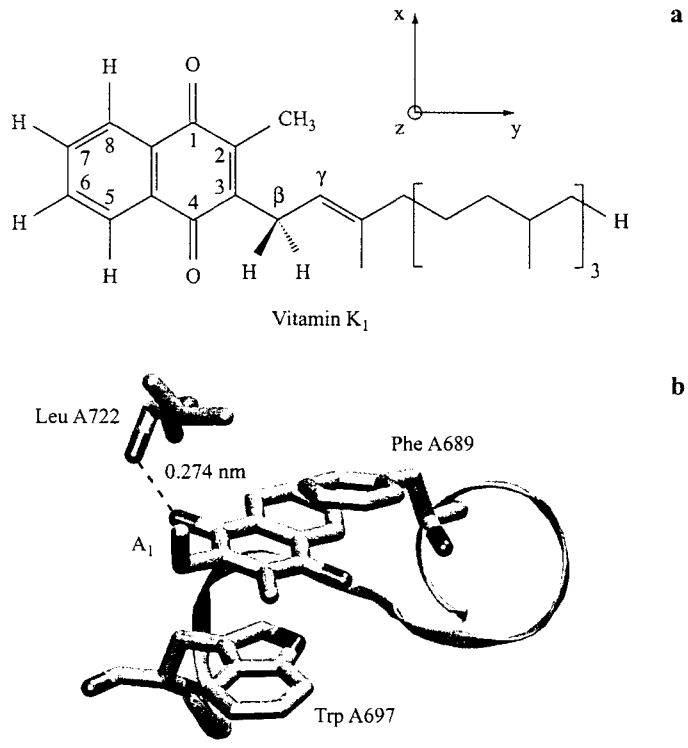

Fig. 1. a Molecular structure and numbering scheme of vitamin K_1 (phylloquinone). The molecular axes system is shown (*z*-axis perpendicular to the π-plane of VK_1 and *x* parallel to the C-O bonds). The *g* tensor axes are assumed to be parallel to the molecular axes, see refs. 20 and 67. **b** Binding site of A_1 in PS I (psaA subunit) from ref. 4 including three surrounding amino acids. Note that the backbone N-H of Leu A722 is in H-bonding distance to the C-O group at position 4 of the VK_1 (0.274 nm). The isoprenoid chain of VK_1 has been truncated for clarity.

ary acceptor $A_1^{\bullet -}$ must be photoaccumulated in prereduced PS I. During this process structural changes of the cofactor and/or the protein cannot be excluded.

However, it has recently been shown that pulse ENDOR spectroscopy can also be performed on the light-generated secondary radical pair $P_{700}^{\bullet +}A_1^{\bullet -}$ [31, 32], which has a lifetime of about 200 μs. This provides the possibility to directly obtain information on the quinone anion radical in the photoactive state on a microsecond time scale avoiding possible effects occurring due to the high pH, the dithionite treatment or the prolonged photoaccumulation procedure. This technique has recently been used to study the native PS I and several pathway mutants containing other quinones and point mutations near the quinone acceptor [33–35].

Here we present a comparison between the secondary acceptor in the photoaccumulated state $A_1^{\bullet -}$ and in the secondary radical pair state $P_{700}^{\bullet +}A_1^{\bullet -}$ by time-resolved pulse ENDOR spectroscopy. Furthermore, the existence of a hydrogen bond

is demonstrated and analyzed by ENDOR. Together with g tensor data from high-field EPR a detailed picture now evolves for the electron acceptor $A_1^{\bullet -}$ in PS I.

2 Materials and Methods

Vitamin K_1 was purchased from Merck and used without further purification. 2-propanol, 1,2-dimethoxyethane (DME) and 2-methyl tetrahydrofurane (MTHF) were obtained from Fluka and were all spectroscopic grade.

The radical anion $VK_1^{\bullet -}$ in 2-propanol was generated by addition of potassium *tert*-butylate in tenfold excess to a 10 mM deoxygenated quinone solution under argon. In ether solution (2:1 mixture of DME-MTHF) the radical anion was generated by potentiostatic coulometry of a 3 mM quinone solution with a tenfold excess of tetra-*n*-butyl ammonium tetrafluoroborate as supporting electrolyte. The electrolysis was performed in a vacuum cell described in ref. 36 and the samples were sealed under vacuum.

The isolation and purification of PS I particles from the cyanobacterium *Thermosynechococcus elongatus* (formerly *Synechococcus elongatus*) is described in ref. 37.

The generation of the radical anion $A_1^{\bullet -}$ in PS I followed a protocol described in ref. 18. Here the PS I particles were prereduced with 30 mM sodium dithionite at pH 10 in the dark at 4°C for 30 min followed by photoaccumulation of $A_1^{\bullet -}$ at $T = 205$ K for 5 min with two 150 W halogen lamps (4 cm water filter, cut-off 750 nm). Under those conditions the formation of other radicals ($A_1^{\bullet -}$) was not detectable for *T. elongatus* [30].

EPR sample preparation and measuring conditions for pulse ENDOR measurements on the secondary radical pair $P_{700}^{\bullet +}A_1^{\bullet -}$ are as outlined in ref. 32. The light-induced radical pair $P_{700}^{\bullet +}A_1^{\bullet -}$ has been created by in situ repetitive laser irradiation of the sample in the microwave (mw) resonator.

The pulse EPR and ENDOR experiments were carried out on a Bruker ESP380E spectrometer with an ESP360D-P ENDOR accessory. The samples were cooled to 80 K with an Oxford helium cryostat (CF935). For the ENDOR experiments on the radicals a Davies-type sequence was used [38]. In situ light excitation was achieved with a Nd:YAG laser from Spectra Physics (GCR 130). The high-resolution continuous-wave (cw) ENDOR and general TRIPLE experiments in liquid solution were performed on a Bruker ESP300 EPR spectrometer equipped with home-built ENDOR accessory described in ref. 39 with an ENDOR resonator of local design [40].

The simulations of the spectra were done with a laboratory-written program on the basis of a second-order perturbation approach [41]. Density functional theory (DFT) calculations were performed on 2-propenyl-3-methyl-naphthoquinone with two water molecules on each carbonyl oxygen as a model for VK_1 in 2-propanol with the program suite Gaussian 98 [42]. After geometry optimization with gradient-corrected exchange-correlation functional B3LYP and a 6-31G(2d, 2p) basis set, hfcs were calculated with the EPR-II basis set.

3 Results and Discussion

3.1 ENDOR Spectroscopy of $VK_1^{\bullet-}$ in Organic Solvents

To determine the isotropic hfc constants (hfcs) high-resolution ENDOR experiments near room temperature in liquid solution were performed for $VK_1^{\bullet-}$. The respective spectrum obtained in 2-propanol at $T = 280$ K is shown in Fig. 2. At low temperature the isoprenoid chain is locked and two hfcs are obtained for

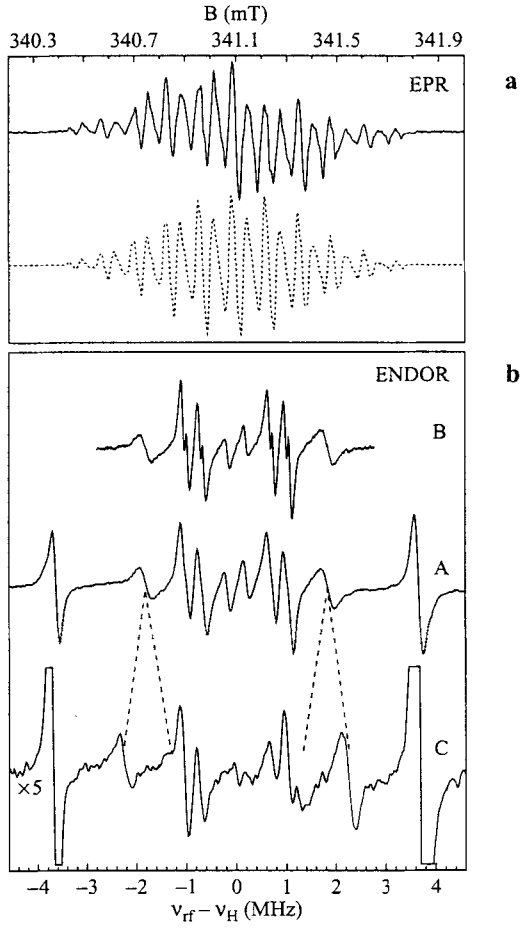

Fig. 2. X-band EPR and ENDOR spectra in liquid solution of $VK_1^{\bullet-}$ in 2-propanol. **a** EPR spectrum at $T = 280$ K, mw power, 0.5 mw; modulation amplitude, 0.011 mT; time constant, 41 ms; scan time, 41 s. For the simulation (dotted line) the hfcs and multiplicities from Table 1 were used. **b** ENDOR spectra. A: mw power, 4 mw; rf power, 70 W; modulation depth, 70 kHz; time constant, 82 ms; total scan time, 40 min; $T = 280$ K. B: central part at higher resolution (modulation depth, 25 kHz). C: spectrum at $T = 220$ K (amplitude ×5). Note that two of the lines in A split due to hindered rotation (as indicated by dashed lines).

Table 1. Isotropic hfc constants of vitamin K_1 radical anion in liquid organic solutions from ENDOR/TRIPLE resonance.[a]

Solvent	Carbon position[b]						
	2	3	6	7	8.5	5.8	3
	CH_3	β-CH_2	α-H	α-H	α-H	α-H	γ-H
2-Propanol[c]	+7.32	+3.65[d]	−2.15	−1.96	−1.48	−1.29	−0.38
DME-MTHF[e]	+7.22	+3.75	−2.03	−2.03	−0.76	−0.76	−0.38

[a] Relative signs from general TRIPLE resonance [66], errors typically ≤0.03 MHz.
[b] For numbering of positions see Fig. 1; assignments are based on sign determinations (α/β protons), dynamic processes (β-H's) and DFT calculations [45].
[c] $T = 280$ K.
[d] At $T = 220$ K the lines split into two line pairs with hfcs of +4.52/+2.47 MHz due to hindered rotation of the isoprenoid chain [44].
[e] $T = 250$ K.

the β-CH_2 protons (Table 1, see also refs. 43 and 44), whereas the other hfcs are only little affected. Very similar hfcs are measured in ether solution (DME-MTHF mixture), see Table 1. The assignment of the α-protons in the benzoic ring is based on DFT calculations [45]. In isotropic solution, interaction with protons in hydrogen bonds cannot be observed [46]. Our data for $VK_1^{\bullet -}$ in alkaline 2-propanol are in agreement with data of ref. 47 and previous measurements [44, 48] in ethanol but deviate from the data given for $VK_1^{\bullet -}$ in *n*-butanol [49]. The reasons for the differing results in ref. 49 are not clear at present.

Solution ENDOR experiments are not possible for the radical ions in PS I since the tumbling of this very large protein (molecular weight of monomeric PS I of about 356000 Da) [4] is too slow at 20°C to average out the anisotropies of the *g* tensor and of most hfcs [50, 51] leading to powder-type spectra even at ambient temperature. Thus, only the low-temperature solid-state pulse ENDOR spectra of $VK_1^{\bullet -}$ can be directly compared. They have the advantage that resonances from purely dipolar interactions with surrounding protons can be observed (e.g., from hydrogen bonds) [52]. Furthermore, the components of the hf tensors are available, e.g., from the magnetically equivalent methyl protons. Only at very low temperatures the free rotation of the methyl group can be stopped [53]. Resonances from the nonmethyl protons are usually more difficult to analyze due to the larger anisotropy and concomitantly larger line width [52].

In Fig. 3 the powder pulse ENDOR spectra of $VK_1^{\bullet -}$ in 2-propanol and DME-MTHF are shown. It is known from EPR measurements in frozen 2-propanol and DME-MTHF [21] that hydrogen bonds are formed in the alcohol, whereas such interactions are absent in the apolar ethers (cf. also refs. 20 and 46). Thus, the simulation has to include a H bond tensor for $VK_1^{\bullet -}$ in 2-propanol but not in DME-MTHF in addition to the tensors of the protons local to the quinone ring (Fig. 3). In Table 2 the ^1H hfc tensor values of the methyl group and the hydrogen bond are compared.

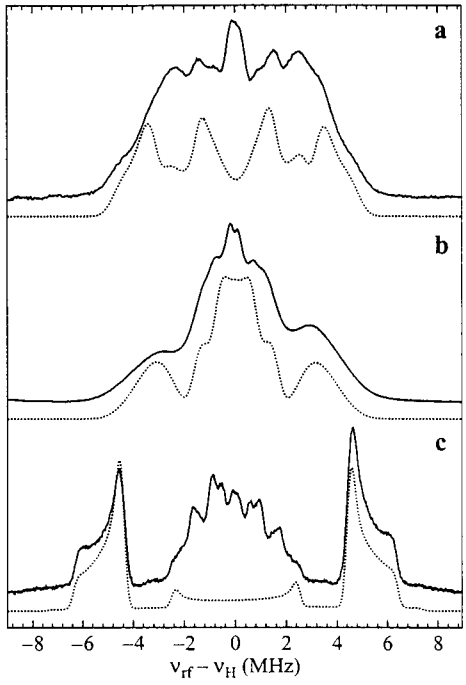

Fig. 3. Comparison of the pulse ENDOR spectrum of $VK_1^{\bullet-}$ in DME-MTHF (2:1 mixture) (**a**) and in 2-propanol (**b**) and of $A_1^{\bullet-}$ in PS I (**c**). All spectra were obtained at the center of the EPR spectrum (no orientation selection). Simulations with the data from Table 2 are given as dotted lines. Experimental conditions: $T = 80$ K, Davies ENDOR sequence ($\pi_{mw} = 128$ ns, $\pi_{rf} = 8$ μs).

Table 2. Principal hfc tensor components of the methyl and the H bond protons of vitamin K_1 radical anion in frozen organic solvents and of the secondary acceptor radical anion $A_1^{\bullet-}$ in the PS I protein ($T = 80$ K).[a]

Species	2-CH_3				H bond	
	A_x	A_y	A_z	A_{iso}	$A_\perp$	$A_\parallel$
$VK_1^{\bullet-}$ in 2-propanol	6.40(5)	9.70(5)	6.70(5)	7.6	(−)2.7(1)	(+)5.7(1)
$VK_1^{\bullet-}$ in DME-MTHF	5.9(1)	9.2(1)	5.9(1)	7.0	—	—
$A_1^{\bullet-}$ photoaccum.	9.10(5)	12.80(5)	8.70(5)	10.2	(−)4.9(1)	—[b]
$A_1^{\bullet-}$ in $P_{700}^{\bullet+}A_1^{\bullet-}$[c]	8.9(1)	12.5(1)	8.9(1)	10.1	(−)4.9(1)	n.d.

[a] Values from spectral simulations (Figs. 3 and 4). Errors in the last digit are given in brackets. The orientation of the methyl hf tensor was rotated by 30° around the g_z axis so that A_y is directed along the C-CH_3 bond. The hf tensor of the hydrogen bond in $VK_1^{\bullet-}$/2-propanol was oriented such that $A_\parallel$ made an angle of 25° with the g_x direction. For $A_1^{\bullet-}$ in the protein the component $A_\parallel$ of the hydrogen additionally makes an angle of 50° with the g_xg_y-plane.

[b] The $A_\parallel$ component of the H bond tensor of $A_1^{\bullet-}$ could not be determined with confidence due to interference of signals from $A_0^{\bullet-}$ (cf. [54]). In ref. 45 a value of (+)14.8 MHz was given (see text).

[c] The hfcs of $A_1^{\bullet-}$ in the radical pair were taken directly from the measured spectrum.

The differences are rather small for the methyl proton hf tensors ($\Delta A_{iso} \approx$ 10%). These deviations can be explained by the very different polarity and H-bond-forming ability of these solvents. H-bonding increases the charge density at the carbonyl oxygens. Thereby the spin density at the oxygens is decreased and this effect leads to an increase of spin density in the ring and thereby to larger proton hyperfine couplings (cf. Table 2). The data for $VK_1^{\bullet -}$ in 2-propanol are in reasonable agreement with those obtained in alkaline ethanol by Rigby et al. [15], who obtained for the methyl protons $A_{||}$ = 10 MHz, $A_{\perp}$ = 6.8 MHz and for the H bond tensor $A_{||}$ = 5.2 MHz and $A_{\perp}$ = 2.2 MHz. From the dipolar tensor measured for the H bond (Table 2) a hydrogen bond length can be estimated from the point dipole approximation [46, 52]. By using an oxygen spin density of $\rho_O^{\pi} = 0.19$ (from ^{17}O labeling experiments of $VK_1^{\bullet -}$ [45]) one obtains $R_{O\text{-}H} \approx 0.175$ nm in good agreement with values for similar quinone radical anions in alcoholic solutions [46] and theoretical estimates [27, 28]).

3.2 ENDOR Spectroscopy of $A_1^{\bullet -}$ Photoaccumulated in PS I

The comparison of the pulse ENDOR spectra of $VK_1^{\bullet -}$ in the organic solvents and $A_1^{\bullet -}$ photoaccumulated in PS I showed major spectral differences of the hf interactions (cf. Fig. 3). In $A_1^{\bullet -}$ the magnitude of the methyl proton tensor is strongly increased, an observation that has previously been reported [15, 30]. This shift of spin density in $A_1^{\bullet -}$ could be attributed to a strong one-sided H bond between the oxygen O_4 of the radical and the protein surrounding that increases the spin density at C_2, the π center adjacent to the coupled methyl group [46, 52].

To obtain information on the exact magnitude of the hf tensors and their orientations with respect to the g tensor frame, orientationally selected pulse ENDOR spectra have been measured across field positions of the EPR envelope. Three spectra are shown as example in Fig. 4 that were taken at the field positions indicated in the EPR spectrum. At position B (center) a powder-type spectrum with little orientational selection is obtained. The spectrum is dominated by one axial hf tensor well separated from the central part and is assigned to the magnetically equivalent protons of the freely rotating methyl group of $A_1^{\bullet -}$. Several smaller hf splittings are observed in the central part of the spectrum that are resulting from the methylene protons, the α-protons of the benzoic ring and possibly from protons of the radical's environment. At field position C (close to g_z) a rather good orientation selection is obtained. Here, g_z is parallel to the plane normal of the π radical. This is also a principal direction (A_z) of the hf tensors, the other two components are lying in the π-plane of the radical. The splittings in the ENDOR spectrum C in Fig. 4 thus directly give A_z (CH_3). At field position A both hf components A_x and A_y of the methyl proton tensor obviously contribute to the spectrum (Fig. 3a).

In the simulations of the orientation selection ENDOR spectra (Fig. 4) only the methyl tensor and a possible H bond tensor were considered. The principal

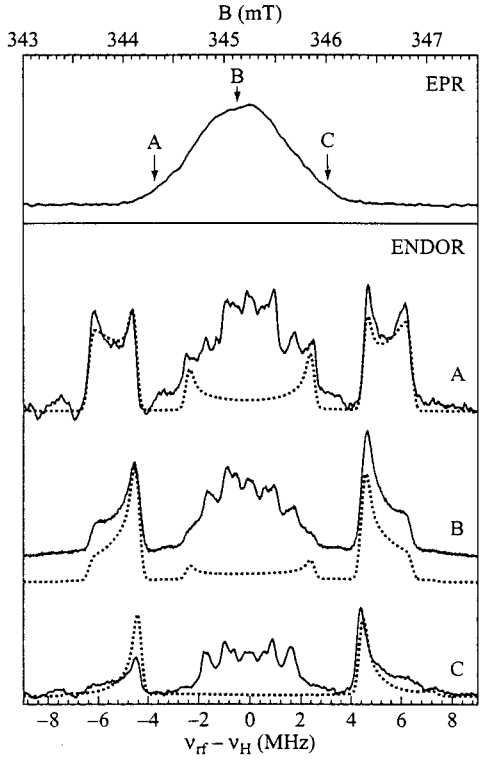

Fig. 4. Field-swept echo EPR spectrum (top) and pulse ENDOR spectra of photoaccumulated $A_1^{\bullet-}$ in PS I at the three indicated field positions A, B, and C indicated in the EPR. Simulations including the methyl and H-bond proton tensors (for details see Table 2) are shown as dotted lines. For experimental conditions see Fig. 2. Note that spectra B are the same as those in Fig. 3c.

values given in Table 2 show that the methyl proton tensor of $A_1^{\bullet-}$ has a rather large anisotropy of $(A_{\parallel} - A_{\perp})/A_{iso} = 0.38$, $(A_{\perp} = (A_x + A_z)/2$, $A_{\parallel} = A_y)$. This was also found for other quinone radicals [46] and is due to the neighborhood of the carbonyl group that carries a large spin density. The tensor somewhat deviates from axial symmetry. The major principal tensor component $A_y \equiv A_{\parallel}$ is found in plane 30±5 degrees off the g_y direction (molecular y-axis, Fig. 1a) and therefore lies along the C(2)-CH_3 bond direction. This is in agreement with the analysis of the EPR spectra of $A_1^{\bullet-}$ at 94 GHz [21, 30]. A_z is oriented to a good approximation perpendicular to the π-plane of the $A_1^{\bullet-}$ and A_x lies in plane perpendicular to A_y. It should be noted that at low temperatures (less than 30 K) spectral changes were observed for the EPR and ENDOR spectrum of $A_1^{\bullet-}$ that dominantly affect the methyl group ^1H hf tensor. This fully reversible effect has been explained by a partial freezing of the methyl group rotation [45].

In principle, the direction of the H bond can be obtained from simulations of orientation-selected ENDOR and high-field EPR spectra. Such an analysis (see,

e.g., Fig. 4) has been attempted and the preliminary simulation data show that the H bond tensor is not lying in the molecular plane of the radical but must occupy an out-of-plane position. Since the EPR spectrum is dominated by the hfc of the methyl group and since there is no significant broadening at any of the principal g values measured at W-band, the hydrogen bond most probably lies 30–60 degrees out off the molecular plane. This agrees with the simulation of the ENDOR spectra (Fig. 4). In the X-ray structure the H bond direction is 33 degrees off the quinone plane [4, 2].

$A_1^{\bullet-}$ has also been photoaccumulated under the same conditions in PS I preparations of *Synechocystis* PCC 6803, spinach and *Chlamydomonas reinhardtii*. Whereas very similar spectra to those of *T. elongatus* were found for *Synechocystis*, the ENDOR spectra for $A_1^{\bullet-}$ of spinach and *C. reinhardtii*, were broad and almost featureless [30, 45]. This is probably due to the fact that they are contaminated by other radicals, e.g., $A_0^{\bullet-}$, a chlorophyll *a* radical anion [30, 45, 54]. Thus, for these species no reliable hfcs could be obtained by this method.

The identification of proton ENDOR resonances of the hydrogen bonds is usually achieved by H-D exchange and by the dipolar character of the hf coupling ($A_{iso} \approx 0$, $A_{||} = -2A_{\perp}$), cf. refs. 46, 52 and 55. However, in case of PS I it turned out that even prolonged incubation in D_2O did not lead to any exchange of the protons in the ENDOR spectrum of $A_1^{\bullet-}$. This could be due to the very hydrophobic binding pocket of A_1 (Fig. 1).

An alternative approach is to exchange the native VK_1 with other deuterated quinones and detect the ^1H ENDOR resonances of $A_1^{\bullet-}$ in this PS I in H_2O buffer. Such experiments have recently been performed with fully deuterated 2-methyl naphthoquinone (vitamin K_3, VK_3) and a species receptive of that. This molecule was incorporated into the A_1 site of a specific deletion mutant (menB, cf. ref. 33) and showed the same geometry as the native VK_1, as demonstrated by transient EPR [56]. The radical also exhibited the same g tensor values as $VK_1^{\bullet-}$ (Table 3) within error ($g_x = 2.0063$, $g_y = 2.0051$, $g_z = 2.0024$) [56]. From the photoaccumulated $A_1^{\bullet-}$ in this PS I preparation a ^1H ENDOR spectrum was obtained [45] lacking the typical strong resonances of the $VK_3^{\bullet-}$ (e.g., from the methyl protons). The observed features are thus assumed to result from the radical's surrounding, in particular the larger couplings are assigned to hydrogen bonds to the carbonyl groups of $A_1^{\bullet-}$. From the prominent features in the spectrum an

Table 3. Principal g tensor values of vitamin K_1 radical anion in frozen organic solvents and in the PS I protein ($T = 80$ K). Errors in the last digit are given in brackets.

Species	g_x	g_y	g_z	g_{iso}	Reference
$VK_1^{\bullet-}$ in 2-propanol	2.00578(3)	2.00503(3)	2.00224(3)	2.00435	21
$VK_1^{\bullet-}$ in *n*-butanol	2.00588	2.00496	2.00225	2.00436	49
$VK_1^{\bullet-}$ in DME-MTHF	2.00623(3)	2.00505(3)	2.00220(3)	2.00449	21
$A_1^{\bullet-}$ in PSI, photoaccum.	2.00625(3)	2.00512(3)	2.00220(3)	2.00452	21
$A_1^{\bullet-}$ in PSI, $P_{700}^{\bullet+}A_1^{\bullet-}$	2.0062(1)	2.0051(1)	2.0022(1)	2.0045	16

axial tensor is deduced (Table 2). Similar resonances between 4.5 and 5.0 MHz are also present and quite pronounced in all $A_1^{\bullet-}$ spectra obtained and in the radical pair spectra (Sect. 3.3) of the native system. This coupling is therefore assigned to the tensor of the proton in a H bond between $A_1^{\bullet-}$ and the protein (probably N-H (Leu), see Fig. 1b). Rigby et al. [15] also reported a hydrogen bond tensor that was obtained from ENDOR/TRIPLE data of $A_1^{\bullet-}$ in PS I of *Anabena variabilis* ($A_{\parallel} = +13.4$ MHz, $A_{\perp} = -5.0$ MHz). These authors postulated that there is a second H bond to $A_1^{\bullet-}$ ($A_{\perp} = -5.8$ MHz). However, the strong spin density shift in the $A_1^{\bullet-}$ ring (see above) and also the X-ray structural data (Fig. 1b) show that only one of the carbonyl groups is hydrogen bonded.

A problem of the above described experiments is that in the photoaccumulated $A_1^{\bullet-}$ state the additional presence of $A_0^{\bullet-}$ (a Chl $a^{\bullet-}$ species) cannot be excluded. For $A_0^{\bullet-}$ in PS I of spinach resonances for the two methyl groups at rings I and IV of Chl *a* in the range of 5.1 to 6.3 MHz and 12.6 to 15.2 MHz, respectively, have very recently been reported [54]. The possible superposition of these pronounced signals makes a reliable analysis of the more weak features arising from the H bond in the ENDOR spectrum of $A_1^{\bullet-}$ very difficult. Since $A_0^{\bullet-}$ is not present in the spectrum of the secondary radical pair $P_{700}^{\bullet+}A_1^{\bullet-}$, the ENDOR analysis of the RP would be very helpful for a final assignment. Such experiments are described in Sect. 3.3.

3.3 ENDOR Spectroscopy of the Radical Pair State $P_{700}^{\bullet+}A_1^{\bullet-}$

In PS I the $A_1^{\bullet-}$ species can be trapped in sufficient yield by prereducing the FeS centers with dithionite that also reduces $P_{700}^{\bullet+}$ at low temperature (about 200 K) after light-induced charge separation [57]. However, this photoaccumulation procedure and the use of a high pH and dithionite might change the structure and/or the electronic interactions in the reaction center and thus the data obtained for $A_1^{\bullet-}$ might deviate from those observed in the native untreated system on a shorter time scale. We have therefore developed a time-resolved pulse ENDOR method that allows the direct observation of $A_1^{\bullet-}$ in the initially formed secondary radical pair state $P_{700}^{\bullet+}A_1^{\bullet-}$ after light excitation (Sect. 2) [9, 31] and a procedure for the analysis of such spectra [32].

A complication arises from the fact that, in principle, an ENDOR response from both radicals, $P_{700}^{\bullet+}$ and $A_1^{\bullet-}$, is obtained. However, the ENDOR effect of isolated $P_{700}^{\bullet+}$ is smaller than that of $A_1^{\bullet-}$ [45]. The experimental conditions for the detection of these species are also somewhat different. Under the conditions used here (pulse separation) the contributions of $P_{700}^{\bullet+}$ to the RP spectrum are minor. Thus, in the ENDOR spectra of Fig. 5, resonances from $A_1^{\bullet-}$ dominate and those of $P_{700}^{\bullet+}$ are suppressed. This becomes evident from a comparison of the ENDOR spectrum of the RP with those of the individual radicals $A_1^{\bullet-}$ (Figs. 3 and 4) and $P_{700}^{\bullet+}$ [51]. A remarkable feature of the ENDOR spectrum of the RP is the occurrence of emissive and absorptive lines, the observed pattern depends on the field position in the EPR spectrum for which the spectrum was obtained.

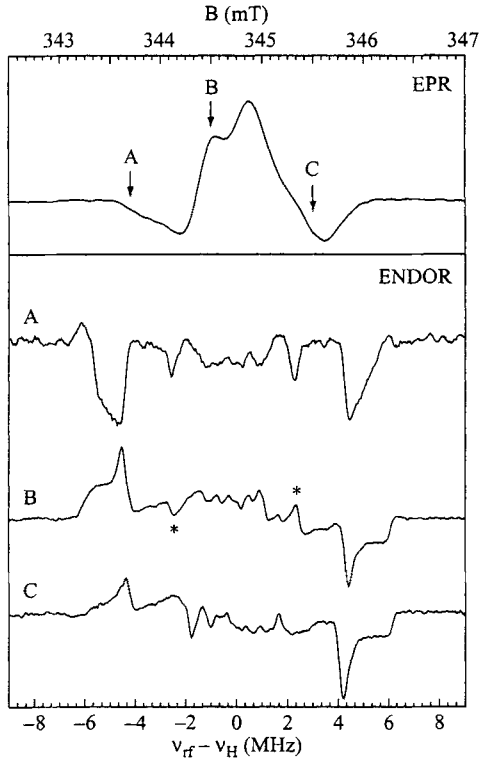

Fig. 5. Field-swept echo EPR (top) and pulse ENDOR spectra A, B, and C of the light-induced secondary radical pair $P_{700}^{\bullet+}A_1^{\bullet-}$ in PS I of *T. elongatus*. The ENDOR spectra A, B, and C were taken at field positions indicated in the EPR spectrum (top). The ^1H ENDOR line pair assigned to the hydrogen bond tensor ($A_\perp$ component) is denoted by asterisks in B. Experimental conditions were the same as in Figs. 3 and 4 with additional laser pulse at 532 nm 500 ns prior to the ENDOR sequence.

In Fig. 5 the field-swept echo (FSE)-detected EPR spectrum of the RP $P_{700}^{\bullet+}A_1^{\bullet-}$ is shown and pulse ENDOR spectra obtained at three different field positions. At the low-field edge (position A), where the EPR is in emission, most of the ENDOR lines are also emissive. With increasing field position the polarization of the low-frequency ENDOR lines changes, they become absorptive, whereas the high-frequency counterpart remains emissive. This is best seen for the large methyl group hf tensor at the spectral wings. Close to the high-field edge of the EPR (position C) the low-frequency part of the ENDOR spectrum becomes weak and almost disappears. These effects can be explained on the basis of the spin-correlated radical pair (SCRP) model [32, 45] and depend on the complicated interplay of the different Larmor frequencies of $P_{700}^{\bullet+}$ and $A_1^{\bullet-}$, the electron spin-spin coupling and the hyperfine coupling. Furthermore, the limited orientation selection at X-band frequencies also contributes to the intensity patterns and line width. Nevertheless, the spectra can be analyzed and this leads to values

for the hf tensor components of $A_1^{\bullet-}$ in the RP (Table 2). The methyl proton tensor shows differences outside the error margins as compared to that measured for the photoaccumulated $A_1^{\bullet-}$. This shows that the latter has a slightly deviating electronic structure that is most probably caused by a relaxation of the radical anion in the protein environment at 200 K that is not occurring at 80 K. The line pair assigned to an hf tensor component of the H bond is also quite prominent in the spectra. An interesting feature is that the polarization pattern for this line (Fig. 5b) is different from that of the methyl group protons indicating a different sign of the hfc [32]. Since no large (negative) α-proton coupling is expected for the radical (cf. Table 1), this finding corroborates the assignment of these resonances to the H bond tensor ($A_\perp$ component).

However, the $A_\parallel$ tensor component indicated in the photoaccumulated spectra of $A_1^{\bullet-}$ (Fig. 4) could not be clearly detected. This makes a final conclusion on the magnitude of this tensor difficult at present. If one assumes that $A_\perp \approx -4.9$ MHz, the tensor is traceless and the oxygen spin density is $\rho_O^\pi = 0.19$ in $A_1^{\bullet-}$, one would obtain a hydrogen bond length of $R_{O\text{-}H} \cong 0.145$ nm from the point-dipole approximation. The expected lowering of ρ_O^π due to H bonding [28] would lead to an even shorter H bond. For such short H bonds the point-dipole approximation leads to erroneous results and is not applicable.

An estimate on the basis of the spin density shift (methyl hfcs) and DFT calculations yielded a H bond length of $R_{O\text{-}H} = 0.155$ nm for $A_1^{\bullet-}$ [45]. Geometry optimization of the binding pocket on the basis of the structure shown in Fig. 1b (DGAUS, BP86 functional, DZVP basis set, ref. 21) yielded a H bond distance of 0.156 nm and an out-of-plane angle of 35° relative to the quinone π-system of $A_1^{\bullet-}$. The respective hf tensor calculated is $A_x = -4.93$ MHz, $A_y = -4.87$ MHz, $A_z = 8.69$ MHz. This shows good agreement with the experimental value of $A_\perp = 4.9$ MHz. From the X-ray structure of PS I in the neutral ground state a H bond distance of 0.174 nm is obtained for A_1. Comparison with the value obtained here for the $A_1^{\bullet-}$ state (about 0.156 nm) indicates a structural change of the binding pocket upon charge separation.

The detection and analysis of $A_1^{\bullet-}$ in the RP state $P_{700}^{\bullet+}A_1^{\bullet-}$ has been used for PS I not only from *T. elongatus* (Fig. 5) but also for the green algae *C. reinhardtii*. $A_1^{\bullet-}$ photoaccumulated in the latter could not be analyzed due to significant contamination with $A_0^{\bullet-}$. The ENDOR experiments on the RP circumvent these difficulties. The hf data for $A_1^{\bullet-}$ of the two PS I systems studied are almost identical showing that A_1 in *C. reinhardtii* has basically the same structure and interaction with the binding pocket as in *T. elongatus*. The technique has been used to study several pathway mutants of *Synechocystis* [33, 58] and A_1-site mutants of *C. reinhardtii* [34, 59].

4 Conclusion

The binding of vitamin K_1 in the PS I protein significantly lowers its midpoint potential. This large change between aqueous phase and protein ($\Delta E_m > 600$ mV)

is caused by the hydrophobic binding pocket of A_1. This pocket completely excludes the intrusion of water, as shown by our H-D exchange experiments. The impact of the surrounding on A_1 is demonstrated experimentally by the large shift of the g tensor (in particular the g_x component) of $A_1^{\bullet-}$ compared to $VK_1^{\bullet-}$ in protic polar solvents (Table 3).

Clearly, the g tensor of a radical ion measured by high-field EPR techniques is a very good indicator for the polarity of the environment [26–28]. $VK_1^{\bullet-}$ in an apolar ether solvent (DME-MTHF) shows g tensor values that are identical to those of $A_1^{\bullet-}$ in PS I [21] (Table 3). The solvent polarity affecting the g tensor is also reflected in the midpoint potential for $VK_1/VK_1^{\bullet-}$. In ethanol, $E_m = -260 \pm 5$ mV, whereas in MTHF, an $E_m = -710 \pm 5$ mV (vs. NHE) is obtained [45]. For $A_1/A_1^{\bullet-}$ in PS I, E_m values in the range of -810 mV [23] to -754 mV [60] were reported. Thus, the value in the apolar nonprotic ether is not too far from the E_m value of VK_1 in the A_1 site of PS I. This shows that the A_1 binding pocket has an extremely low polarity index [45].

Nevertheless, the VK_1 in the PS I binding pocket has one hydrogen bond to its carbonyl oxygen O_4. The existence of such a H bond is obvious from the X-ray crystallographic structure of PS I [4], and its impact on the electronic structure of $A_1^{\bullet-}$ is clearly demonstrated by the large changes observed for the spin density distribution for $VK_1^{\bullet-}$ in and outside the protein. On the basis of our preliminary assignment of the tensor of the H-bonded proton in $A_1^{\bullet-}$ a short and quite strong bond is concluded. This H bond is probably changing its strength when A_1 accepts the electron. Such changes have been discussed in detail for the bacterial reaction center [52]. It is important to note that this single H bond has only a minor effect on the g values as was derived from DFT calculations [27, 28]. This bond is holding the VK_1 in place and is probably also necessary to stabilize the negative charge to a certain extent. The unusual binding of a quinone via a single one-sided hydrogen bond has recently also been discussed for ubiquinone QH in the enzyme ubiquinol oxidase [61].

Hydrogen bonding has been discussed to play an important role in proton-coupled electron transfer processes [62–64]. In this respect it is interesting to know the extent of delocalization of the electron onto the surrounding amino acids for the involved cofactors. For $A_1^{\bullet-}$ it has been found that a small fraction of the spin/charge density is delocalized via the H bond to the peptide backbone, which is manifested by the detection of a hyperfine coupling of the nitrogen (^{14}N) of the leucine Leu A722 [25]. In that work, by ESEEM techniques, a second ^{14}N coupling could be detected and can now be assigned to the tryptophan Trp A697 that is π-stacked to the quinone (cf. Fig. 1b). Together with the phenylalanine Phe A689 this residue constitutes the tightly packed very hydrophobic binding site of A_1.

At present the information on the hydrogen bond ^1H hfc tensor magnitude of $A_1^{\bullet-}$ and its geometry is incomplete. Attempts to fully determine this tensor and the other hfcs of the radical by orientationally selected pulse ENDOR at higher mw frequencies are currently under way in our laboratory. Experiments performed on the RP state will advantageously be used to analyze the electronic

structure of $A_1^{\bullet-}$ in different species without contamination of $A_0^{\bullet-}$. As an additional probe to measure the geometry of H bonds to quinone radical anions the deuterium quadrupole coupling detected by ^2H ENDOR at higher mw frequencies has recently been introduced [28, 65]. This interaction will also be employed for the detailed analysis of the interactions and bonding situation of radicals like $A_1^{\bullet-}$ in PS I in future experiments.

Acknowledgements

This work is dedicated to Y. N. Molin and Y. D. Tsvetkov on the occasion of their 70th birthday. The PS I samples of *T. elongatus* were obtained from P. Fromme (Technische Universität Berlin). The PS I sample of *Synechocystis* with d_8-$VK_3^{\bullet-}$ incorporated was provided by J. Pushkar (Freie Universität Berlin) in a joint project with J. Golbeck (Penn State University Park, Pennsylvania, USA) H. Zimmermann (Max-Planck-Institut, Heidelberg) and D. Stehlik (Freie Universität Berlin). We thank F. Lendzian (Technische Universität Berlin) and F. MacMillan (Universität Frankfurt/Main) for experimental support and for helpful discussions. The work was supported by Deutsche Forschungsgemeinschaft (Sfb 498 and Priority Program SPP 1051) and Fonds der Chemischen Industrie (WL).

References

1. Blankenship R.E.: Molecular Mechanisms of Photosynthesis. Oxford: Blackwell Science Ltd. 2002.
2. Fromme P., Jordan R., Krauß N.: Biochim. Biophys. Acta **1507**, 5–31 (2001)
3. Brettel K., Leibl W.: Biochim. Biophys. Acta **1507**, 100–114 (2001)
4. Jordan R., Fromme P., Witt H.T., Klukas O., Saenger W., Krauß N.: Nature **411**, 909–917 (2001)
5. Joliot P., Joliot A.: Biochemistry **38**, 11130–11136 (1999)
6. Guergova-Kuras M., Boudreaux B., Joliot A., Joliot P., Redding K.: Proc. Natl. Acad. Sci. USA **98**, 4437–4442 (2001)
7. Webber A.N., Lubitz W.: Biochim. Biophys. Acta **1507**, 61–79 (2001)
8. Vassiliev I.R., Antonkine M.L., Golbeck J.H.: Biochim. Biophys. Acta **1507**, 139–160 (2001)
9. Bittl R., Zech S.G.: Biochim. Biophys. Acta **1507**, 194–211 (2001)
10. van der Est A.: Biochim. Biophys. Acta **1507**, 212–225 (2001)
11. Deligiannakis Y., Rutherford A.W.: Biochim. Biophys. Acta **1507**, 226–246 (2001)
12. Rigby S.E.J., Evans M.C.W., Heathcote P.: Biochim. Biophys. Acta **1507**, 247–259 (2001)
13. Bonnerjea J., Evans M.C.W.: FEBS Lett. **148**, 313–316 (1982)
14. Thurnauer M.C., Gast P.: Photochem. Photobiol. **9**, 29–38 (1985)
15. Rigby S.E.J., Evans M.C.W., Heathcote P.: Biochemistry **35**, 6651–6656 (1996)
16. van der Est A., Prisner T., Bittl R., Fromme P., Lubitz W., Möbius K., Stehlik D.: J. Phys. Chem. B **101**, 1437–1443 (1997)
17. Zech S., Hofbauer W., Kamlowski A., Fromme P., Stehlik D., Lubitz W., Bittl R.: J. Phys. Chem. B **104**, 9728–9739 (2000)
18. MacMillan F., Hanley J., van der Weerd L., Knüpling M., Un S., Rutherford A.W.: Biochemistry **36**, 9297–9303 (1997)
19. Hales B.J.: J. Am. Chem. Soc. **97**, 5993–5997 (1975)
20. Burghaus O., Plato M., Rohrer M., Möbius K., MacMillan F., Lubitz W.: J. Phys. Chem. **97**, 7639–7647 (1993)
21. Teutloff C., Hofbauer W., Zech S.G., Stein M., Bittl R., Lubitz W.: Appl. Magn. Reson. **21**, 363–379 (2001)

22. Vos M.H., Gorkum H.J.: Biochim. Biophys. Acta **934**, 293–302 (1988)
23. Sétif P., Bottin H., Brettel K. in: Current Research in Photosynthesis (Baltscheffsky M., ed.), vol. 2, pp. 539–546. Dordrecht: Kluwer Academic 1990.
24. Swallow A.J. in: Function of Quinones in Energy Conserving Systems (Trumpower B.L., ed.), pp. 59–72. New York: Academic 1982.
25. Hanley J., Deligiannakis Y., MacMillan F., Bottin H., Rutherford A.W.: Biochemistry **36**, 11543–11549 (1997)
26. Knüpling M., Törring J.T., Un S.: Chem. Phys. **219**, 291–304 (1997)
27. Kaupp M., Remenyi C., Vaara J., Malkina O.L., Malkin V.G.: J. Am. Chem. Soc. **124**, 2709–2722 (2002)
28. Sinnecker S., Reijerse E., Neese F., Lubitz W.: J. Am. Chem. Soc. **126**, 3280–3290 (2004)
29. Nimz O., Lendzian F., Boullais C., Lubitz W.: Appl. Magn. Reson. **14**, 255–274 (1998)
30. Teutloff C., MacMillan F., Bittl R., Lendzian F., Lubitz W. in: Photosynthesis: Mechanisms and Effects (Garab G., ed.), pp. 607–610. Dordrecht: Kluwer Academic 1998.
31. Bittl R., Zech S.G., Teutloff C., Krabben L., Lubitz W. in: Photosynthesis: Mechanisms and Effects (Garab G., ed.), pp. 509–514. Dordrecht: Kluwer Academic 1998.
32. Fursman C.E., Teutloff C., Bittl R.: J. Phys. Chem. B **106**, 9679–9686 (2002)
33. Zybailov B., van der Est A., Zech S.G., Teutloff C., Johnson T.W., Shen G., Bittl R., Stehlik D., Chitnis P.R., Golbeck J.H.: J. Biol. Chem. **275**, 8531–8539 (2000)
34. Boudreaux B., MacMillan F., Teutloff C., Agalarov R., Gu F., Grimaldi S., Bittl R., Brettel K., Redding K.: J. Biol. Chem. **276**, 37299–37306 (2001)
35. Xu W., Chitnis P., Valieva A., van der Est A., Pushkar Y.N., Krzystyniak M., Teutloff C., Zech S.G., Bittl R., Stehlik D., Zybailov B., Shen G., Golbeck J.H.: J. Biol. Chem. **278**, 27864–27875 (2003)
36. Lendzian F., Plato M., Möbius K.: J. Magn. Reson. **44**, 20–31 (1981)
37. Fromme P., Witt H.: Biochim. Biophys. Acta **1365**, 175–184 (1998)
38. Davies E.R.: Phys. Lett. A **47**, 1 (1974)
39. Rautter J., Lendzian F., Lubitz W., Wang S., Allen J.P.: Biochemistry **33**, 12077–12084 (1994)
40. Zweygart W., Thanner R., Lubitz W.: J. Magn. Reson. A **109**, 172–176 (1994)
41. Gessner C.: Ph.D. thesis, Technische Universität Berlin, Berlin, Germany, 1996.
42. Frisch M.J., Trucks G.W., Schlegel H.B., Scuseria G.E., Robb M.A., Cheeseman J.R., Zakrzewski V.G., Montgomery J.A., Stratmann R.E., Burant J.C., Dapprich S., Millam J.M., Daniels A.D., Kudin K.N., Strain M.C., Farkas J.T.O., Barone V., Cossi M., Cammi R., Mennucci B., Pomelli C., Adamo C., Clifford S., Ochterski J., Petersson G.A., Ayala P.Y., Cui Q., Morokuma K., Malick D.K., Rabuck A.D., Raghavachari K., Foresman J.B., Cioslowski J., Ortiz J.V., Baboul A.G., Stefano B.B., Liu G., Liashenko A., Piskorz P., Komaromi I., Gomperts R., Martin R.L., Fox D.J., Keith T., Al-Laham M.A., Peng C.Y., Nanayakkara A., Gonzalez C., Challacombe M., Gill P.M.W., Johnson B.G., Chen W., Wong M.W., Andres J.L., Head-Gordon M., Replogle E.S., Pople J.A.: Gaussian98, Revision A.6. Pittsburg, Pennsylvania: Gaussian, Inc. 1998.
43. Fritsch J.M., Tatwawadi S.V., Adams R.N.: J. Phys. Chem. **71**, 338–342 (1967)
44. Das M.R., Connor H.D., Leniart D.S., Freed J.H.: J. Am. Chem. Soc. **92**, 2258–2268 (1970)
45. Teutloff C.: Ph.D. thesis, Technische Universität Berlin, Berlin, Germany, 2003.
46. MacMillan F., Lendzian F., Lubitz W.: Magn. Reson. Chem. **33**, S81–S93 (1995)
47. MacMillan F.: Ph.D. thesis, Freie Universität Berlin, Berlin, Germany, 1993.
48. Barry B.A., Bender C.J., McIntosh L., Ferguson-Miller S., Babcock G.T.: Isr. J. Chem. **280**, 129–132 (1988)
49. Bowman M.K., Thurnauer M.C., Norris J.R., Dikanov S.A., Gulin V.I., Tyrishkin A.M., Samoilova R.I., Tsvetkov Y.D.: Appl. Magn. Reson. **3**, 353–368 (1992)
50. Chasteen N.D., Francavilla J.: J. Phys. Chem. **80**, 867 (1976)
51. Käss H., Fromme P., Witt H.T., Lubitz W.: J. Phys. Chem. B **105**, 1225–1239 (2001)
52. Lubitz W., Feher G.: Appl. Magn. Reson. **17**, 1–48 (1999)
53. Clough S., Poldy F.: J. Phys. Chem. **51**, 2076–2084 (1969)
54. Rigby S.E.J., Muhiuddin I.P., Santabarbara S., Evans M.C.W., Heathcote P.: Chem. Phys. **294**, 319–328 (2003)
55. O'Malley P.J., Chandrashekar T.K., Babcock G.T. in: Antennas and Reaction Centers of Photosynthetic Bacteria (Michel-Beyerle M.E., ed.), pp. 339–344. Berlin: Springer 1985 (Springer Series in Chemical Physics, vol. 42)

56. Pushkar Y.N., Zech S.G., Stehlik D., Brown S., van der Est A., Zimmermann H.: J. Phys. Chem. **106**, 12052–12058 (2002)
57. Gast P., Swarthoff T., Ebskamp F.C.R., Hoff A.J.: Biochim. Biophys. Acta **722**, 163–175 (1983)
58. Sakuragi Y., Zybailov B., Shen G., Jones A.D., Chitnis P.R., van der Est A., Bittl R., Zech S., Stehlik D., Golbeck J.H., Bryant J.A.: Biochemistry **41**, 394–405 (2002)
59. Redding K., Bittl R., MacMillan F., Teutloff C., Gu F., Grimaldi S., Boudreaux B. in: PS2001 Proceedings of the 12th International Congress on Photosynthesis. Melbourne: CSIRO Publishing 2001.
60. Iwako M., Itoh S.: Plant Cell Physiol. **35**, 98–993 (1994)
61. Grimaldi S., Ostermann T., Weiden N., Mogi T., Miyoshi H., Ludwig B., Michel H., Prisner T.F., MacMillan F.: Biochemistry **42**, 5632–5639 (2003)
62. Tommos C., Babcock G.T.: Biochim. Biophys. Acta **1458**, 199–219 (2000)
63. Okamura M.Y., Paddock M., Graige M.S., Feher G.: Biochim. Biophys. Acta **1458**, 148–163 (2000)
64. Remy A., Gerwert K.: Nat. Struct. Biol. **10**, 637–644 (2003)
65. Flores M., Isaacson R., Calvo R., Feher G., Lubitz W.: Chem. Phys. **294**, 401–413 (2003)
66. Kurreck H., Kirste B., Lubitz W.: Electron Nuclear Double Resonance Spectroscopy of Radicals in Solution: Application to Organic and Biological Chemistry. Weinheim: VCH Verlagsgesellschaft 1988.
67. Isaacson R.A., Lendzian F., Abresch E.C., Lubitz W., Feher G.: Biophys. J. **69**, 311–322 (1995)

Authors' address: Wolfgang Lubitz, Max-Planck-Institut für Bioanorganische Chemie, Stiftstrasse 34-36, 45470 Mülheim an der Ruhr, Germany